

Analysis of Spatial Patterns of Phase in Neocortical Gamma EEGs in Rabbit

Walter J. Freeman and John M. Barrie

Department of Molecular and Cell Biology

University of California at Berkeley, California 94720-3200

Journal of Neurophysiology 84: 1266-1278, 2000

Running title: Phase patterns in neocortical EEG

Keywords: EEG, gamma oscillations, EEG phase gradients, neurodynamics, phase cones, state transitions

ABSTRACT

Arrays of 64 electrodes (8x8, 7x7 mm) were implanted epidurally on the surface of the visual, auditory or somatosensory cortex of rabbits trained to discriminate conditioned stimuli in the corresponding modality. The 64 EEG traces at all times displayed a high degree of spatial coherence in wave form, averaging >90% of the variance in the largest PCA component. The EEGs were decomposed with the FFT to give the spatial distributions of amplitude and phase modulation (AM and PM) in segments 128 ms in duration. Spatial (2-D) and temporal (1-D) filters were designed to optimize classification of the spatial AM patterns in the gamma range (20-80 Hz) with respect to discriminative conditioned stimuli. No evidence was found for stimulus-dependent classification of the spatial PM patterns. Instead, some spatial PM distributions conformed to the pattern of a cone. The location and sign (maximal lead or lag) of the conic apex varied randomly with each recurrence. The slope of the phase gradient varied in a range corresponding to that of the conduction velocities of axons reported to extend parallel to the cortical surfaces. The durations and times of recurrence of the phase cones corresponded to those of the optimally classified spatial AM patterns. The interpretation is advanced that the phase cones are manifestations of state transitions in the mesoscopic dynamics of sensory cortices, by which the intermittent AM patterns are formed. The phase cones show that the gamma EEG spatial coherence is not due to volume conduction from a single deep-lying dipole generator, nor to activity at the site of the reference lead on monopolar recording. The random variation of the apical sign shows that gamma AM patterns are self-organized and are not imposed by thalamic pacemakers. The half-power radius of the phase gradient provides a useful measure of the soft boundary condition for the formation and read-out of cooperative cortical domains responsible for binding sensory information into the context of prior experience in the process of perception.

INTRODUCTION

Five premises are adopted here for analysis of the spatiotemporal integration of neural activity within and between areas of neocortex. First, neurons communicate with each other over short distances by ionic diffusion of synaptic neurotransmitters/modulators, and over long distances only by propagated action potentials that incur delays. This premise disallows appeals to instantaneous communication by ephaptic linkages through fields of electrical current (Terzuolo and Bullock 1956; Bullock 1997; Bullock et al. 1995; Prechtl, Bullock and Kleinfeld, 2000), electromagnetic resonance (Adey 1969, 1993), or quantum coherence (Hameroff 1998). Second, communication between parts of neurons is predominantly by ionic loop current, which is governed by the cable equation, and which, like diffusion, imposes attenuation of amplitude with distance (Hodgkin and Rushton 1946). Local sources of energy for the action potential surmount this attenuation, but at the cost of distance-dependent delay. Therefore, neurons that are distributed in a network or mass and that fire simultaneously can achieve

simultaneity in the arrival times of their action potentials at selected points in the network only under severe constraints. Third, spatiotemporal integration of the activity of afferent axons by the cable-like dendrites of receiving neurons requires some degree of synchrony in the multiple inputs. This means that some component of the activity of each of the transmitting axon terminals must be at or near zero time lag with respect to the activity of all. The span for "zero lag" is defined here as the modal duration of an action potential, ~ 1 ms, and "near" as the duration of a passive membrane time constant, $\sim \pm 5$ ms.

Fourth, synchronization is essential for integration of the activity of 'feature detector' neurons in the process of perception, whereby the action potentials of relay neurons that are activated by sensory neurons having receptor fields for features of a stimulus are combined to form a representation of the entire stimulus. How much synchrony is required, and how is it achieved in the face of axonal delays? This constitutes what has been called the 'binding problem' (Milner 1974; von der Malsburg 1983; Singer 1993; Hardcastle 1994; Schillen and König 1994). When the problem is formulated in this way, the description of the neural mechanism requires measurement of that fraction of the variance of the activity of individual neurons or local ensembles that is covariant over the whole network or mass. The solution also requires an explanation of how that fraction of the total variance that is covariant over the ensemble can constitute or carry a neural signal, and a description of a neural mechanism by which that covariant fraction can be extracted by the target neurons receiving spatial activity distributions that have been transmitted by axons with obligatory propagation delays.

The fifth premise is that the activity of cortical neurons is synchronized by their synaptic interaction in closed loops. Anatomical evidence shows that each neuron forms synapses on thousands of others within its axonal arbor and receives axon terminals from thousands of other neurons within its dendritic arbor, but cell counts indicate that each neuron connects only with on the order of 1% of the neurons that lie within its reach. Anatomists such as Sholl (1956) and Braitenberg and Schüz (1991) have concluded that the likelihood of a feedback connection between any designated pair of neurons may be as low as one in a million. If the connections of most neurons are as sparse as these estimates indicate, and if the impact of single action potentials is as minute with respect to the thresholds for neural firing of recipient neurons as estimated by biophysicists (Amit 1989), one of the feedback loops by which each neuron can interact with other neurons is provided by its local neighborhood. This premise complements the significant roles of interactions among delimited subsets of neurons forming discrete networks in information processing (Jagadeesh, Gray and Ferster 1992; Arieli et al. 1995; Tsodyks et al. 1999; Zhu and Connors 1999; Nicolelis 1997; Nicolelis et al. 1998), which can give rise to 'zero lag' correlations between the gamma oscillations of neurons separated by millimeter distances (Roelfsema et al. 1997), despite the axonal transmission times that are expected to cause phase shifts between oscillations. Usher, Schuster and Niebur (1993) and Schillen and König (1994) have modeled this phenomenon by assuming that the feedback delay within each target matches the transmission delay between targets in an excitatory feedback network. Traub et al. (1996) have overcome some of the rigidity of those models by invoking doublet firing of single neurons (Freeman 1975), which they show is enhanced in states of high amplitude gamma.

The fifth premise provides an alternative mechanism for spatiotemporal integration in cortex through a distinction between the *microscopic* functions of individual neurons and the *mesoscopic* functions of neural masses in local neighborhoods (Freeman, 2000), reserving the term *macroscopic* to refer to the much larger ensembles that are visualized with whole brain imaging techniques such as fMRI, SPECT and optical recording (Arieli et al. 1995). The dendritic currents of cortical neurons give rise to extracellular fields of potential, which, owing to the laminar architecture of cortex, sum in the volume conductor and constitute the main source of the electroencephalogram (EEG). These are the same currents that determine the firing probabilities of the neurons (Freeman 1975; Nunez 1981; Mitzdorf 1985, 1987; Freeman

,1992). This causal relation is manifested in the statistical dependence of pulse probability of cortical neurons conditional on the amplitude of the EEG in the same local neighborhood (Freeman 1975; Eeckman and Freeman 1990). The relation is weak, because approximately 10,000 pulses are required from each individual neuron in the local mass to reveal the statistical regularity (Freeman 1992). Estimates of the fraction of the variance of individual spike trains that is covariant within an ensemble of simultaneously recorded cortical spike trains are on the order of 0.1% (Aertsen et al. 1989; Abeles 1991).

The mesoscopic EEG activity that results from distributed synaptic interactions in each local neighborhood provides a measure of the local mean field intensity of that neighborhood. What makes the EEG important is that while it is the local average of electric potentials established by the vector sum of currents across the cortical impedance, that sum is the reflection of the mesoscopic state formed by the cooperative actions that result from synaptic interactions, mainly by excitatory synapses on excitatory neurons that are broadly but sparsely distributed. A counterexample is a compound nerve action potential formed by the sum of action potentials triggered by an electrical stimulus of a peripheral nerve. It spreads with time and distance forming the 'A' and 'C' peaks, because the axons do not interact to bind together the action potentials. The currents sum in the volume conductor, but they do not reveal a local mean field, because the axons do not interact. Moreover, in cortex the EEG currents are too weak to influence directly the firing rates of the individual neurons (Freeman, 1962, 1975, 1992; Freeman and Baird, 1989). The cooperative interactions that are revealed by the EEG typically are aperiodic oscillations in the spectral range from 1 to 100 Hz with intermittent peaks in well known ranges labeled theta, alpha, beta, gamma, etc. The FFT (Press et al. 1988) of relatively long epochs of recording (> 1 s) yields spectra that show a near linear fall in log power with increasing log frequency at a slope near 2, a " $1/f^2$ " distribution that is characteristic of Brownian motion and telegraph noise. Short segments (< 0.1 s) typically reveal at least one spectral peak at a frequency that differs seemingly at random in successive segments. This variation reflects the frequency modulation and aperiodicity that characterize the neocortical EEG.

Simultaneous recordings of EEG from 8x8 electrode arrays (7x7 mm) placed subdurally on the visual, auditory or somatosensory cortices of trained rabbits have revealed a high degree of spatial coherence in these spatial windows as previously reported (Freeman and Viana Di Prisco 1986; Barrie et al. 1996). After temporal bandpass filtering to extract the activity in the gamma range (20-80 Hz in the waking rabbit), on average $>90\%$ of the variance was found to be contained in the first component of principal components analysis (PCA), as compared with $\sim 50\%$ when EEGs were recorded simultaneously from multiple areas and filtered in the same way. The shared gamma wave form in trained rabbits revealed spatial distributions of amplitude modulation (AM) in short time segments. These segments were classifiable with respect to conditioned stimuli (CSs) that the rabbits had been trained to discriminate (reinforced CS+ from unreinforced CS-) in the sensory modality corresponding to the cortex under observation (Barrie et al. 1996). Therefore, they were identified as "AM patterns".

The spatial coherence and the relatively narrow spectral peak of the carrier wave in the gamma range in these same brief AM patterns have made it possible using the FFT to measure the phase of the EEG at 64 sites in short time segments with respect to the phase of the spatial ensemble average of the 64 traces at the shared peak frequency. The square of the cosine of the phase for each trace gives a basis for estimating its level of shared variance with respect to the whole. The present report describes the spatial patterns of phase modulation (PM) that have been found in the EEGs from the primary sensory cortices, an interpretation of the mechanism by which the PM patterns form, and a suggestion on how the spatial patterns are transformed by output pathways and received by the targets of transmission. Note should be taken that every multichannel EEG segment of any length gives an amplitude distribution and a phase

distribution; the term "pattern" is reserved here for AM patterns that can be classified with respect to CSs, and for PM patterns that correspond to the direction and conduction velocities of axons in a specific tract in the brain (Bressler 1987), or that can be fitted with a cone over time durations corresponding to the time durations of AM patterns, as determined by classification efficacy (Fig. 10 in Barrie et al. 1996).

These AM and PM patterns provide crucial evidence that the spatially coherent wave form of the epipial EEG is not due to a deep-lying generator having a broad point spread function (PSF, a term used in optics to denote the distribution in a plane of observation of light from a point source), nor is it due to oscillation in potential at the reference lead in monopolar recording, but instead to an array of equivalent point dipoles in a plane at some depth below the plane of recording (Freeman, 1975). Direct measurement of the PSF is an arduous task that has only been done for the olfactory bulb, but equivalent information can be obtained from the spatial spectrum of the EEG, and this has been done for the bulb, prepyriform, visual, auditory and somatic cortices in rabbits, and the superior temporal gyrus in humans (Freeman et al., 1999).

MATERIALS AND METHODS

Chronic implantation of an epidural electrode array. Eighteen female New Zealand White (NZW) rabbits (2.5-4.5 kg, ~ 2 years old) were implanted (aseptically, full surgical anesthesia by 4% isoflurane / O₂ mixture) with a prefabricated electrode array onto the left hemisphere. Arrays were 0.25 mm- stainless steel wires in an 8x8 square matrix (0.79 mm interelectrode distance to limit spatial aliasing, 7x7 mm window). Reference and ground leads were placed in the skull adjacent to the site of each placement over the visual, auditory, somatic or olfactory cortex. The arrays were placed in accordance with descriptions of the locations of the primary sensory neocortices in rabbits by means of mapping with evoked potentials (Galli et al. 1971; Hollander and Halbig 1980; McMullen and Glaser 1982; Gould 1986). Subjects were maintained 2-4 years, then sacrificed with 120 mg/kg pentobarbital, perfused with 10% formalin, and autopsied. All procedures were conducted according to protocols approved by the University of California at Berkeley Animal Care and Use Committee with veterinary supervision by the Office of Laboratory Animal Care.

Experimental paradigm. For recording each subject was placed into a restraining carrier in an electrically shielded, sound-resistant dark chamber. The electrodes were connected to World Precision Instruments ISO 4/8 differential amplifiers. A pneumograph was attached to the chest, skin clips for the US were placed onto the left cheek, and white noise (72 dB) was introduced into the chamber. After 3 weeks of familiarization, each subject was trained using classical aversive conditioning to discriminate between two stimuli corresponding to its implant site: one of two 10 ms full-field flashes varying only in intensity (3.6 vs. 2.8 ft.-cd); or binaural (stereo earphones at 72-84 dB above the 72 dB white noise) 100 ms sinusoidal tones at 500 vs. 5000 Hz); or a 3 second air puff onto the cheek vs. the hindquarters (Barrie et al. 1996). One of the conditioned stimuli (designated CS+) was reinforced with a weak electric shock to the cheek adjusted initially to elicit an orienting response (Freeman and Viana Di Prisco 1986), and the other conditioned stimulus (designated CS-) on randomly interspersed trials was not reinforced. For each experiment forty 6-second artifact-free EEG records were recorded, filtered with single-pole, first-order RC filters (6 dB/octave falloff) at 100 Hz (3 dB point) and 0.1 Hz, digitized at 500 Hz, phase corrected for the time lag introduced by multiplexing (10 μ s), and digitally stored to magnetic disk in binary data files (~16 MB/file). Each record was divided into a 3-second prestimulus period and a 3-second poststimulus period. The sequence of CS+/CS- trials (20 each) was randomized across the set of 40 trials, and the time interval between each stimulus was randomized between 30 and 120 seconds. Three replicates were made for each experiment (Barrie et al. 1996).

Data analysis.

All data analysis was done off-line on a Macintosh PowerPC using original software specifically developed for this purpose. Every data set was reviewed and edited for bad recording channels and EEG artifacts (bad connections, animal movement, 60 Hz noise).

EEG records were segmented by either of two methods. The first method involved using a sliding window to parse each record into m overlapping, 128 ms EEG segments (where w indexed each segment) separated by 2 ms intervals (Barrie et al. 1996). Each individual 128 ms EEG segment was then converted into a root-mean-square (RMS) spatial AM distribution, after bandpass filtering (at the optimal bandpass filter setting), resulting in a series of 1 x 64 column vectors (\bar{V}),

$$\bar{V} = R_e \quad e \in \{1,2,\dots,64\} \quad (1)$$

where R is the RMS amplitude of the EEG for each channel (e).

The second method was based on locating stable phase cones in the spatial distributions of phase of neocortical EEGs. Conic phase patterns had been found in EEGs of the olfactory bulb (Freeman and Baird 1987; Freeman 1990). Here each multichannel EEG record was parsed into m overlapping, 128 ms segments separated by 2 ms intervals. Each segment was decomposed by fast Fourier transform (FFT, Press et al. 1988), into 50, 64-dimensional spatiotemporal distributions of phase (\bar{P}) at fixed frequency intervals (f) ranging from 2-100 Hz. Phase differences in (\bar{P}) at high spatial frequencies were inferred to be due to noise (Fig. 6 in Freeman and Viana Di Prisco 1986), so they were attenuated with a spatial filter in each 8x8 phase distribution by transforming the frame into the frequency domain with the 2-D FFT (embedding in a matrix of 32x32 zeroes and omitting Hamming and Hanning), passing the real and imaginary components through digital 2-D highcut and lowcut filters (Freeman and Baird 1987; Barrie et al. 1996), and using the inverse 2-D FFT to recover the smoothed values. The two optimal cutoff frequencies in cycles/mm were determined by repetition to give a tuning curve (Fig. 1) to identify the value giving the most conic-like phase segments. A low cutoff spatial filter was used to minimize the risk of what appeared to be an artifact from excessive highcut filtering, and to take advantage of the usefulness already demonstrated of spatial bandpass filtering (Freeman and Baird 1987). Each spatially filtered phase distribution was then fitted by nonlinear regression with a 2-D conic surface (\bar{C}) in planar coordinates,

$$\bar{P}_{w,f} = \left\{ P_{e,f}^{(w)} : w = 1,2,\dots,m; f = 2,4,\dots,100; e = 1,2,\dots,64 \right\} \quad (2)$$

$$\bar{P}_{w,f} \quad \bar{C}_{w,f} \quad \varphi(\bar{P}_{w,f})$$

where P is the spatial phase distribution, w is the window index (for m windows), f is the frequency index, e is the electrode array channel index, \bar{P} is the 1x64 phase vector, \bar{C} is the 1x64 cone vector representing the conic pattern, and φ is the conic function regressed onto the phase distribution. Every cone had a slope, b (in mm/radian) and an apex (location in x and y mm from the center of the recording array) which was not restricted within the area of the recording area. The residual between the original phase distribution and the conic regression was minimized by nonlinear regression,

$$R_{w,f} = \left(\bar{P}_{w,f} - \bar{C}_{w,f} \right) / \bar{P}_{w,f} \quad w \in \{1,2,\dots,m\}, f \in \{2,4,\dots,100\} \quad (3)$$

and expressed as the percentage of total power for each frequency and segment. Since every 128 ms EEG segment contained a phase distribution at 50 different frequencies, the regressions with large residuals (meaning the original phase distribution did not resemble a cone) were removed by flagging all apices of cones with low residuals. If there were multiple peaks in the phase pattern (at a single frequency) then the residual of the conic regression increased (i.e., bad fit and no cone is identified). There could be multiple, simultaneous phase cones existing at different frequencies. For example, there could be a conic phase pattern at 10 Hz and another conic phase pattern at 40 Hz. However, all attempts to fit the sum of 2 conic surfaces to phase distributions at a single frequency resulted in singular matrices, that is, nonlinear regression failed.

Conic apices were separated into two categories: apices with < 20% residual (\bar{A}),

$$\bar{A}_{w,i} = \text{apex}(\bar{C}_{w,f}) \quad w \in \{1,2,\dots,m\}, f \in \{2,4,\dots,100\}, i \in \{1,2,\dots,n_w\}; \text{ where } R_{w,f} < 20\% \quad (4)$$

and apices with < 40% residual (\bar{A}),

$$\bar{A}_{w,j} = \text{apex}(\bar{C}_{w,f}) \quad w \in \{1,2,\dots,m\}, f \in \{2,4,\dots,100\}, j \in \{1,2,\dots,n_w\}; \text{ where } R_{w,f} < 40\% \quad (5)$$

The numbers of apices within each segment from conic regressions with $R < 20\%$ and $R < 40\%$ were recorded as n_w and n_w , respectively. Both matrices of apices were subsequently sorted from lowest to highest residual (i.e., $\bar{A}_{1,1}$ indexed the apex of the phase cone with the lowest residual below 20% within the first segment). Such a categorical division was empirically used in order to demarcate the beginning (always a cone with $R < 20\%$) and ending (always a cone with $R > 40\%$) of particular segments of temporally contiguous phase cones with apices that are constant in location and sign (i.e., “phase segments”) (Barrie et al. 1996).

Once all of the individual phase patterns resembling cones were located and marked (by Eq. 4 and Eq. 5), the search for phase segments began. This strategy had two parts: the location of the initial site of nucleation (this was always a cone with $R < 20\%$) and the location of subsequent temporal points (always consecutive phase cones with $R < 40\%$) which were indicative of the temporal duration of a cortical event. After locating the initial point, called the site of nucleation, two distances were calculated,

$$A_1 = \|\bar{A}_{w,i} - \bar{A}_{w+q,j}\| \quad i \in \{1,2,\dots,n_w\}, j \in \{1,2,\dots,n_{w+q}\} \quad (6)$$

and

$$A_2 = \|\bar{A}_{w+q,j} - \bar{A}_{w+q+1,k}\| \quad j \in \{1,2,\dots,n_{w+q}\}, k \in \{1,2,\dots,n_{w+q+1}\} \quad (7)$$

The first distance indicated how far (in mm) an apex (located $2q$ ms in time from the initial phase cone) was from the initial site. The second distance indicated how far any two consecutive phase cones were from each other. Three criteria were used to identify whether a sequence of phase cones formed a continuous segment that began at $\bar{A}_{w+0,i}$: $A_1 < 1.2$ mm, which constrained an entire sequence of cones within a segment to a particular area of the cortex; $A_2 < 0.5$ mm, which ensured that successive cones lay close to the previous location;

and uniformity in the signs of the slopes of a group of phase cones, all of which had to be either lead or lag. If all of the above criteria were satisfied for $q = 25$ contiguous time steps ($t = 50+$ ms), then a stable phase segment was demarcated. In summary, a stable phase segment was defined as a pattern of phase that had $R < 20\%$ at time $t = 0$, no shift in location > 1.2 mm from the initial point, an apex which did not move > 0.5 mm during any 2 ms interval, and a phase value at the apex that was either positive or negative for the entire $2q$ ms segment. Stationarity over the measurement window is empirically fulfilled because we are able to track similar patterns across 2 millisecond epochs. Fig. 5B illustrates the search for stationary phase segments. The first point (i.e., phase cone apex) within the grouping labeled 'Segment I' represents the site of nucleation. Each subsequent point is located at 2 ms intervals and satisfies all of the above criteria until the spatial jump into the positive quadrant; that was the end of the first stable phase segment. A $1 \times q$ vector (\vec{Z}) demarcated each stable phase segment,

$$\vec{Z}_{r,s} = T_{r,w+t} \quad r \in \{1,2,\dots,40\}, s \in \{1,2,\dots,N_r\}, t \in \{0,1,\dots,q\} \quad (8)$$

where T was the time in milliseconds beginning at window w and extending to window $w + q$ (the time when no further phase cones could be found to satisfy the above search criteria), for each phase segment (s) within every experimental record (r). There were N_r individual segments per record. Each of these segments was then converted into a series of RMS spatial AM patterns (as in Eq. 1).

To determine whether the demarcated phase segments recurred in specific time intervals with respect to the CSs, a histogram (\vec{H}) of the phase segments was composed for the incidence in the 6 s trials over the 40 trials in each session:

$$\vec{H} = \sum_{r=1}^{40} \sum_{s=1}^{N_r} \vec{Z}_{r,s} \quad (9)$$

By calculating the FFT of \vec{H} , a spectrum of frequencies was computed, reflecting the mean recurrence rates of stable phase cones.

Two other important values obtained by this analysis included the EEG phase velocity (S) in $M \text{ sec}^{-1}$,

$$S \text{ M sec}^{-1} = \left(b \text{ mm rad}^{-1} \times 2\pi f \text{ rad sec}^{-1} \right) / 1000, \quad (10)$$

where b is the slope of the conic surface regressed onto the phase distribution decomposed at frequency f , and the modal diameter (D) in cm is defined as twice the distance from the apex to the half-power level of the EEG:

$$D \text{ M} = S \text{ M sec}^{-1} \times 0.25 \text{ cycle} / f \text{ cycle sec}^{-1}. \quad (11)$$

The absolute phase difference of the oscillation at the common frequency increases monotonically from 0° at the apex with increasing distance of the recording site. The fall in amplitude of the common component is given by the cosine of the phase. At some distance the commonality must fall to zero, and in fact the correlation between simultaneous recordings from different primary sensory cortices is much less than that within each cortex, indicating that each domain of spatial coherence must have a soft boundary. We estimate the location of

the boundary from the radius where the absolute phase difference has increased to 45° , where the cosine is 0.707, and the power of the shared wave form has decreased to the square of the cosine, 0.5.

After an experiment had been segmented (by either fixed-length windows separated by fixed-length time intervals (Barrie et al. 1996) or by locating segments demarcated by stable phase cones) into a matrix of spatial AM pattern vectors, a method of cross-classification was employed to determine whether or not the CS- patterns were significantly different from the CS+ patterns. Briefly, for contiguous temporal epochs, all patterns within that epoch were grouped as either type A (CS-) or B (CS+). Each type was further subdivided into equal groups A₁, A₂, B₁, B₂; the first and second halves of group A/B became subgroups A₁/B₁ and A₂/B₂, respectively. The patterns within the first two subgroups (A₁, B₁) were averaged to form centroids and the Euclidean distance was measured in 64-space from the two centroids to each of the patterns remaining in the second two subgroups (A₂, B₂). If a pattern was closer to its centroid than to the opposite centroid (i.e., a pattern from subgroup A₂ was closer to centroid A₁ than it was to centroid B₁.) then it classified correctly. This classification was repeated by calculating centroids from the second two subgroups and classifying the patterns from the first subgroups. A binomial probability pattern was used to determine whether or not a certain level of classification was significant. This method yielded a time series of probability values showing the times when the CS- and CS+ spatial AM patterns could or could not be separated.

RESULTS

Paleocortical vs. neocortical EEGs. Since the goal of this research was to assess a method, originally used to characterize the EEG from the olfactory system (Freeman and Baird 1987), for parsing the neocortical EEG, a comparison of the characteristics of the olfactory and neocortical EEG was compiled as a reference. The olfactory EEG was strongly correlated to the respiratory rhythm of each rabbit (Fig. 2A, upper). It was punctuated by a sequence of high frequency (20-80 Hz), high amplitude bursts typically referred to as gamma oscillations (Fig. 2B, left). Such olfactory bursts were time-locked to the inhalation phase of the respiratory cycle and were separated by 1/f-type (20-100 Hz), broad spectrum interbursts. Previous research utilized the presence of these gamma bursts as an EEG marker for stimulus-induced, endogenously generated events (Freeman 1978; Freeman 1991). A cursory comparison of the olfactory and visual cortical EEG revealed significant differences. The visual EEG was not correlated to the respiratory rhythm (Fig. 2A, lower), did not have a distribution of gamma oscillations, and only contained an evoked potential marking the arrival time (3000 ms) of the afferent volleys of action potentials into the cortex from the periphery. An examination of the average frequency spectra of visual cortical neuroactivity further demonstrated that (Fig. 2B, right) log power was uniformly distributed across the temporal spectrum as a $1/f^m$ function of log frequency. This relation also held for the spatial spectra (Barrie et al. 1996).

Measurement of AM patterns in neocortices. One property that the olfactory and neocortical EEGs shared was the presence of a common carrier wave at any one instant. This meant that the frequency spectrum of the EEG using the FFT was spatially coherent across the cortex (over distances covered by the 7x7 mm arrays) at any one time. Coherence was revealed by a complex wave form shared on the multiple EEG traces having a common instantaneous frequency, that changed continually and unpredictably. Short time segments (64-256 ms) had prominent peak frequencies, which changed in successive segments, reflecting a continuous modulation in frequency and/or phase. Power spectral analysis of longer segments usually revealed a broad " $1/f^m$ " power spectral density, in which log power decreased linearly with increasing log frequency at slope $m \sim 2$.

Spatial coherence observed in plots of multiple time series (Fig. 3A) was supported by the incorporation of >90% of the variance in the first component of PCA (Barrie et al. 1996). The frequency spectra of averages of EEG segments had a 1/f distribution, but the spectra for individual EEG segments typically centered around one frequency relative to the overall spectra (Barrie et al. 1996). That frequency component revealed spatial amplitude modulation (AM) over the 64 channels in a spatial distribution. Owing to the high covariance of the 64 traces the same AM distribution was found in the root mean square amplitudes. Each AM distribution could be represented by a contour plot (Fig. 3B) and also by a point in n-space, where n was the number of electrodes and EEG traces. Similar AM distributions formed clusters of points in n-space, and multiple AM distributions gave a set of clusters. Assignment of each segment to a class was based on the Euclidean distance of its point to the center of gravity of the nearest cluster.

The AM patterns were modified by classically conditioning the animals to respond to stimuli in the cortex of the corresponding modality; for example, animals with implants over the primary visual cortex (V1) (Thompson et al. 1950; Hollander and Halbig 1980; Hughes and Vaney 1982) received visual stimuli. As the animals were trained to discriminate between one reinforced conditioned stimulus (CS+) and another unreinforced (CS-), new AM patterns appeared and prior patterns were subtly altered. After completion of training, the AM patterns reappeared upon delivery of the corresponding stimuli to which the animals had learned to respond. The locations and durations in time of the AM patterns in neocortical EEGs were not visible as an amplitude modulation over time. The most effective method for detecting them was to pass a moving window, 64-256 ms in duration, in 2 ms steps along the set of 20 CS+ trials and 20 CS- trials, and to determine when the AM patterns differed significantly between the CS- and the CS+ trials. The 64-256 ms duration sliding window was only used for data exploration. The 128 ms window length was most effective and was used throughout this manuscript. The shorter window lengths did not have enough spectral resolution for successful phase segment tracking. The longer window lengths yielded unsatisfactory results, possibly because the longer windows included EEGs that were unrelated to the activity being tracked (i.e., noise was included in the FFT decomposition of the EEG). The binomial probability of a difference by chance offered a convenient measure for when the two sets of distributions differed. As shown in Fig. 4, the AM patterns distinguishing CS+ and CS- trials occurred shortly after the arrival of the CS and at irregular intervals a few hundred milliseconds thereafter.

This statistical assay, which served effectively to classify AM patterns from visual, auditory, somatic or prepyriform cortical EEGs, did not serve to locate the AM patterns in time on *single* trials. The decline in significance of AM pattern separation with elapsed time from the stimulus presentation indicated that the locations in time of successive events varied across trials. The cortical distribution of phase modulation (PM) at the same frequency was given by the FFT. The PM distributions were measured in the same stepped windows in order to determine whether they could be localized on single trials.

Measurement of PM patterns in neocortices. The discovery of PM patterns was based upon the finding of spatially coherent oscillation in multichannel EEGs with spectra in simultaneously recorded short segments having local maxima at the same frequency somewhere in the gamma range. We restricted the selection of the local spectral peak to the gamma range of 20 - 80 Hz, because this was the spectral range in which the AM patterns could be classified with respect to CSs (Fig. 9 in Barrie et al., 1996). The spatial coherence was demonstrated by use of PCA to extract the dominant component for pattern classification on every data set (Fig. 8 in Barrie et al., 1996), in order to show that the results of classification were the same using RMS, FFT, or PCA amplitudes. All of the cortical areas showed that the dominant component captured between 90% - 98% of the total variance despite the lack of zero lag synchrony (Fig. 3A), with no significant differences between areas. The 64

spectra of the EEG traces correspondingly had peaks at the same frequency even as that frequency shifted unpredictably from one segment to the next. Therefore, when that frequency was identified, or when any other frequency was selected, the 64 phase values defined at that frequency provided a spatial phase distribution constituting phase modulation (PM) about the phase of the spatial ensemble average. Comparisons could then be made between PM distributions from differing cortices in search of varieties of PM patterns. Stable patterns of phase had already been identified in the prepyriform cortical EEGs, which were clearly determined by the velocities and directions of propagated action potentials in the lateral olfactory tract (Boudreau and Freeman 1963; Bressler 1987; Bressler 1995). Comparable phase patterns were sought in EEG segments from the primary sensory neocortices, first by visual inspection of contour plots of phase in search of regularities, and next by attempts to find distinctive locations of peaks of phase lead on CS+ *versus* CS- trials on the assumption of topographic organization of activity driven by thalamic pacemakers. Peaks were occasionally found, but the locations varied unpredictably and without relation to CSs, and when they were present in the array the sign varied seemingly at random.

Then a plane was fitted to the 8x8 phase values in search of broad phase gradients such as those found in array recordings of scalp EEGs (Walter 1953) and MEGs (magnetoencephalograms, Llinás and Ribary, 1993), on the premise that large wave fronts might be approximated by a plane with no curvature over the local 7x7 mm covered by the epidural arrays. The phase gradients in some segments did appear to conform to a plane, but the orientation and steepness varied randomly. The patterns were eventually resolved by fitting a cone to the 64 values of phase, giving consistently lower residuals than a plane fitted to the same phase data, and allowing a close fit to the phase extrema that happened to be located within the arrays. The FFT of the 64 traces (128 ms windows stepped at 2 ms intervals) yielded the spatial distributions of amplitude (Fig. 3B) and phase (Fig. 3C) at frequencies in the gamma range. Conic functions were fit (in planar coordinates) to each phase distribution (Fig. 3D) after bandpass filtering (0.2-0.5 c/mm) of the phase values, by which the Standard Error of Measurement of phase was minimized (Fig. 6 in Freeman and Viana Di Prisco, 1986). A phase cone apex was flagged (Fig. 5A) when the variance incorporated by the fitted conic surface exceeded 80% of the total variance. That conic pattern was tracked in successive window steps (defined by Eqs. 4-5) as illustrated in Fig. 5B. PM patterns lasting more than 25 steps (50 ms) were labeled as *stable phase cones*. The distributions that could be fitted with a plane could be explained as having conic apices located well outside the arrays. No significant differences were seen in PM patterns from the three neocortical sensory areas. The relative constancy of the sign of the phase extremum, and of its location, and of the frequency at which the phase was defined, together constituted evidence for stationarity of the dynamic states over the time durations shown in Fig. 7A. Stationarity is defined here to mean cortical dynamics holding in an attractor basin between two successive state transitions, irrespective of the oscillations within that basin, including the trajectories of entry and exit.

The locations and signs of the apices of successive stable phase cones varied unpredictably without relation to the CSs. The duration of identified stable phase cones averaged 80 ms with a long tailed distribution. Neocortical phase velocities in M/s (Eq. 10) had skewed distributions from 0.5 - 4.0 M/s (Fig. 5C). The modal value of 0.6-2.1 M/s was consistent with measurements reported on the conduction velocity of large groups of cortical axons parallel to the pia. No attempt succeeded to define edges of the coherent domains, so an appropriate criterion of size was adopted: the half power diameter across the apex ($\pm \cos 45^\circ$), using Eq. 11. Diameter values were skewed from 5 - 20 mm or more with a mode near 0.5 cm (Fig. 5D).

The dependence of phase lag in radians on the distance between recording electrodes in millimeters was first found without spatial filtering by calculating the absolute phase differences between channels at all frequencies in many windows and many trials. In prior measurements of PM patterns in the olfactory bulb, the conic basis function led to an invariant

measure, which was the steepness of the phase gradient expressed in M/s (Freeman and Baird 1987). The gradients were measured in radians/mm, and they varied with frequency, but when they were converted to M/s by use of the frequency of the oscillation (Eq. 10), they converged to the conduction velocity estimated for the axons of the bulbar axon collaterals running parallel to the surface of the bulb. A similarly invariant relationship was found in EEGs from the prepyriform cortex (Boudreau and Freeman, 1963), so it was sought in the EEG data from the neocortices. Unlike the invariant relation for the olfactory bulb, the phase velocity of the neocortical EEG increased on average with increasing frequency. The breakdown by frequency of the distributions of phase velocities on conversion to M/s using Eq. 10 is shown in Fig. 6 (upper frames) and Table 1 for three frequency bands. The modal phase velocities were consistent with the conduction velocities reported for short intracortical axons over distances up to 3 mm, as distinct from corticocortical, callosal and efferent axons that are much faster (Swadlow and Weyand 1981; Langdon and Sur 1990; Lohmann and Roerig 1994; Swadlow 1994). In the neocortical EEGs a new invariant was found in the modal half-power diameter (Eq. 11) of the identifiable stable phase cones across neocortical locations and frequency bands (Table 1; Fig. 6, lower frames).

Stable phase cones identified by these criteria were found at irregular intervals throughout each trial (Fig. 7A). Pre- and post-stimulus time histograms of the stable phase cones showed higher than average probabilities of cones after the time (3000 ms) of stimulus arrival (Fig. 7B). The FFT of histograms calculated from all neocortices yielded peaks in the 4-8 Hz range (Fig. 7C-E) indicating a degree of rhythmicity in the theta range for the arrival and duration times of stable phase cones. The AM patterns were derived from segments demarcated by stable phase cones in visual, auditory and somatic EEGs as in Fig 3B. These AM patterns also revealed a significant level of correct classification of CS+ and CS- trials, and in comparison to the fixed steps, the AM patterns accompanying stable phase cones gave higher levels of significance later in trials (Fig. 8A-C), indicating that detection of phase cones improved the identification of the locations of behaviorally significant EEG events in the CS - CR interval.

DISCUSSION

EEGs were measured by decomposing them with appropriate basis functions, which in the present case were cosines giving the phase and amplitude of frequencies in the gamma range. Whereas accurate measurement of amplitude was relatively easy, measurement of the phase was subject to large errors of measurement, owing to the brief duration of segments, the small number of cycles in each segment, the strong tendency to FM and AM about center frequencies in both time and space, and the mix of multiple frequencies in spectra of most segments, especially from neocortices with their tendency to "1/f²" spectra. The standard error of measurement was estimated by measuring cosines at unit amplitude and zero phase embedded in varying levels of random numbers to simulate white noise (Freeman and Viana Di Prisco 1986). The results gave standard deviations averaging $\pm 60^\circ$ for raw EEGs, which were reduced to $\pm 6^\circ$ after application of appropriately designed spatial and temporal filters.

The requirement for validating the measurements of spatiotemporal AM patterns was met by relating them to behavior. This criterion led step by step (Freeman 1975; Freeman and Schneider 1982; Freeman 1992; Barrie et al. 1996) to decomposition of EEG time series with cosine basis functions, measurement of AM and PM patterns having the same instantaneous frequency in the arrays, and classification of the AM distributions with respect to sets of CS+ and CS- trials after discriminative conditioning. The PM patterns consistently failed to classify with respect to locations and signs of apices, but the AM patterns extracted from the segments demarcated as stable phase cones did classify well above chance levels at intermittent times between the CS and CR onsets.

The main problem encountered in correlation of neocortical EEGs with behavior (as compared with olfactory EEGs) was temporal segmentation. The identification of spatial AM patterns in olfactory EEGs was facilitated by the prominent respiratory wave in the theta range and the associated temporal AM of the gamma activity giving "bursts" of oscillation. In contrast, visual inspection of the neocortical EEGs gave no indication of where the stationary segments might start or end, either by any near-periodic wave in the theta and alpha ranges, or by any temporal AM in the gamma range. Therefore, a fixed-duration segment was stepped along the multiple EEG traces on every trial, and classifications of AM or PM patterns from CS+ and CS- trials were made between segments on different trials all from the same time step with respect to stimulus onset. The results showed that the selection of AM patterns that was guided by determination of the temporal locations of the stable phase cones improved the reliability of segment classification in the CS-CR intervals. The consistency and reliability of the results from olfactory, visual, auditory and somatosensory EEGs led to the conclusion that the radial phase gradients are not an artifact of the measurement algorithms, and that they manifest an important biophysical property of the neural masses that generate the gamma oscillations of the EEG.

Several inferences follow from this conclusion. First, the common wave form on the 64 electrodes cannot be ascribed to activity at the site of the reference electrode on monopolar recording, or to volume conduction from a deep dipole generator far under the array, not only because of the amplitude modulation [which might conceivably be explained by local variations on cortical specific resistance] but also because of the phase modulation [the reactive component of the cortical impedance vector is much too low to give the observed range of differences - Freeman, 1975]. Nor is it due to decorrelation with distance over a distribution of noise generators smeared by volume conduction (Elul 1972), because that would not give radial phase gradients. Nor does it manifest entrainment of coupled oscillators, because the phase gradients persist through the segments, probably owing to the sparseness (Braitenberg and Schüz 1991) of the local connection densities, which fails to support convergence of activity into synchrony.

Second, the findings can explain the zero time lag correlation reported between the pulse trains of neurons separated by distances less than the array size (König and Schillen 1991; Engel et al. 1992; Singer 1993; Gray 1994; Brosch et al. 1995; Roelfsema et al. 1997), when that relation has been derived between pulse trains of pairs of neurons by time ensemble averaging over multiple trials. When the technique is used because there are too few pulses on any one trial, the unpredictable variation in location and sign of the conic apices randomizes the phase relations on repeated single trials, and the resulting average can only approach zero.

Third, the random variation of the sign of the apices cannot be explained by an intracortical or thalamic pacemaker, because those drivers could only give apices with phase lead whether acting by excitation or inhibition. It is compatible with a symmetry breaking state transition such as a saddle node bifurcation. The property of mesoscopic states that makes them interesting is the capacity they give to an ensemble of neurons for rapid changes in the global spatiotemporal distributions of organization and function of ensembles. Some well known examples are the transitions between waking and sleeping states, between vocalizing and swallowing, and between walking and running, by which the neurons distributed in the brain and spinal cord shift their firing from one coordinated pattern to the next globally in a few ms.

We postulate that in primary sensory cortices a state transition is enabled by a volley of action potentials on afferent axons, which is initiated by a sensory event and gated by thalamic relay nuclei. Gated input transiently increases the level of activity in the cortex. Owing to the asymmetry of the sigmoid curve governing the output of the cortical neurons receiving the volley (Freeman, 1992), the forward gain (sensitivity of the trigger zones of the excited neurons) is increased. Owing to the predominance of intracortical excitatory synapses to other

excitatory neurons, the triggered output goes mainly to excite those other neurons and sensitize them as well. In the ensemble some of the activity returns to the initially excited neurons, still further increasing their activity and sensitivity. This constitutes regenerative feedback at the mesoscopic level that is equivalent to the nonlinear local response of axons approaching their thresholds (Hodgkin and Rushton, 1964). Just as microscopic axons are bistable (either above or below threshold - Izus, Deza and Wio, 1998), we infer that mesoscopic ensembles of cortical neurons are bistable or polystable. Above some threshold an ensemble can become unstable and jump into a high intensity oscillatory state. Owing to the amplitude-dependent gain of the population (Freeman, 1992) the pattern generated in the new stable state that has been triggered by the input is dominated by the intracortical synaptic connections, which are subject to modification by learning during previous experience (Emery and Freeman, 1969), particularly at the excitatory synapses on the dendritic spines of excitatory neurons as described by Rall (1995) and others. Hence the AM patterns could reflect the past and present contexts imposed by behavioral constraints, not the specific forms imposed by the sensory input volley. This could explain the fact that the AM patterns are not invariant with respect to the stimuli, but are modified by new learning, such as that which occurs with changes in reinforcement contingencies (Freeman and Grajski, 1987; Freeman, 1991).

Fourth, evidence from physical distributed systems shows that state transitions do not start simultaneously throughout the systems but begin at a *site of nucleation* and spread radially, as in the formation of a snowflake around a dust particle. The velocity of spread indicated by the radial phase gradient is compatible with the conduction velocities reported for axons running parallel to the pia (Swadlow and Weyand, 1981; Langdon and Sur, 1990; Lohmann and Roerig, 1994; Swadlow, 1994). Those axons extending more than a millimeter (Hellwig, 1993; Read et al., 1997) could play an important role, because there is insufficient time to allow for serial multisynaptic transmission over the predominantly short axons (Sholl, 1956) to the distances covered by observed phase cones. We infer that the phase cones manifest a group property, the velocity of a state transition, not a transfer of information (Freeman, 1990). Physicists call the spread of change at different velocities in media *anomalous dispersion*. An example is hitting a metal rod on one end with a hammer; the sound wave gets to the other end of the rod before the impulse does. Anomalous dispersion in the cerebral cortex may account for the rapidity with which state transitions can spread over large distances faster than can be achieved by serial synaptic transmission, relying instead on small percentages of long axons in corticocortical projections, and on the extreme sensitivity of the cortical ensemble as it approaches the border of its existing basin of attraction, analogous to the 'local response' that sensitizes axons brought near threshold (Hodgkin and Rushton, 1946). We conclude that the radial phase patterns in the EEG provide strong evidence that AM patterns form by self-organizing cortical state transitions that direct the cortices through a landscape of attractors, each yielding a reproducible AM pattern (Freeman, 1992; Freeman et al., 1995).

Fifth, the delays in axonal propagation manifested in the phase cones may serve to delimit the spatial boundaries of neocortical AM patterns during both construction and read-out. The neocortical neuropil forms a continuous sheet, as shown by the phenomenon of spreading depression of Leão (Bures et al. 1974), which stops only at the borders of the neocortex with the archicortex and the callosum. The submillimeter microscopic architecture of cortex is spatially coarse-grained by its input projections into cortical columns and barrels, which are smaller by an order of magnitude than the mesoscopic AM patterns. The EEGs of cortical areas that are separated by macroscopic distances lack high spatial coherence, giving evidence that the mesoscopic AM patterns must have soft boundaries. The obligatory axonal propagation delays may provide the neocortical dynamic boundary conditions, which are required to give the different areas a degree of autonomy, while not freezing them into anatomically fixed arrangements. Within each area the spatially coherent EEGs manifest cooperative interactions among millions of neurons, but cooperativity must weaken with phase dispersion. The radial phase gradients can serve to attenuate mesoscopic synaptic interactions

with distance. With no hard edges the half-power radius ($\pm \cos 45^\circ$) can serve to define the functional boundaries and sizes for local cooperative domains, at the interface between microscopic neural activity and cortical mesoscopic states. The cosine values then provide the desired measure of the degree of relatedness of the gamma activity throughout a temporal segment of the EEG in a mesoscopic cortical area.

Sixth, the classification of AM patterns with respect to CSs reveals that the classificatory information is homogeneously distributed in space; no recording channel in an array is any more or less important than any other (Barrie et al. 1996). This property shows that the information relating to the topographic mapping of the sensory input has been spatially disseminated by the dynamic operation of constructing AM patterns. The independence of the mesoscopic pattern from the details of the input-dependent cortical architecture may be critical for the integration of multisensory percepts, in which the local space-time gradients peculiar to the retinal, cochlear and cutaneous mappings are no longer relevant. This operation also pertains to the read-out of AM patterns. The olfactory bulb transmits through the divergent-convergent lateral olfactory tract that imposes a spatial integral transformation. Each bulbar neuron disseminates its pulses broadly, and each target neuron integrates over input from a wide area of the bulb. This operation sums only the transmitted activity having minimal frequency and phase dispersion, and it attenuates the activity that is not spatially coherent. In effect, it defines the self-organized bulbar mesoscopic activity as signal, and the sense-dependent microscopic activity as noise. Whether the outputs of neocortical primary sensory cortices likewise undergo spatial integral transformation is unknown, but the fact that the neurons in the secondary sensory areas have very large receptor fields gives evidence that a comparable mesoscopic operation may be performed on the outputs of neocortices. In effect, every local population sends the same signal to all targets of a transmitting cortex, in the manner that each fragment of a broken hologram has the entire picture, and each receiving target selects what is appropriate to it. An alternative hypothesis, holding that discrete microscopic networks of selected neurons embedded in the neuropil have been synthesized by large local synaptic modifications during learning, suffers from combinatorial explosions in matching input and output topographic maps, and it does not readily offer a neural code that is common to all perceptual ports beyond the early stages of sensory information processing but prior to multisensory percept formation.

The prepyriform cortex provides an important exception, because its phase gradients are not conic but conform instead to the propagation delays imposed by the directions and velocities of the axonal branches in the lateral olfactory tract, or occasionally to axonal projections in the opposite direction (Freeman 1973; Freeman 1999). This finding indicates that this cortex lacks the autonomous dynamics required for the self-organization of AM patterns and is directly driven by the bulb (Boudreau and Freeman 1963; Bressler 1987). This difference offers a distinction between two types of cortex, one that constructs AM patterns, the other that integrates them selectively. These two types may work pairwise in reciprocity. They might be sought among neocortical areas by measurement of their PM patterns, so that their respective roles might be better understood.

Acknowledgments

This research was supported by the National Institute of Mental Health Grant MH06686 and the Office of Naval Research Grant N00014-90-J-4054. The authors thank Mark D. Lenhart for his invaluable assistance with the surgical procedures and with the experimental paradigm. More information on the background and research interests of the authors may be obtained from the W.J. Freeman Lab WWW server by accessing: <http://sulcus.berkeley.edu> on the Internet.

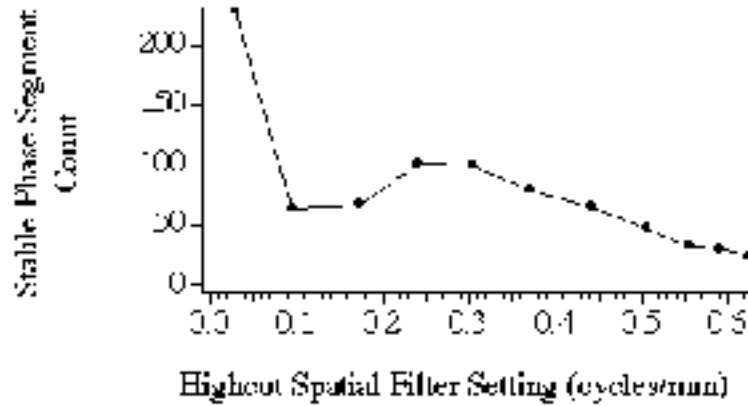
Variable List

\bar{V}	1 x 64 RMS amplitude column vector (\bar{V})
R	RMS amplitude of the EEG for each channel
e	EEG recording channel index
\bar{P}	spatial phase distribution
w	window index
m	number of overlapping, 128 ms EEG windows separated by 2 ms intervals
f	frequency index
\bar{C}	1x64 cone vector representing the conic pattern regressed onto the phase pattern
φ	conic function regressed onto the phase distribution
\bar{A}	apices of conic regressions with < 20% residual
\bar{A}	apices of conic regressions with < 40% residual
n	numbers of apices within each segment from conic regressions with $R < 20\%$
n	numbers of apices within each segment from conic regressions with $R < 40\%$
i	index
j	index
A_1	distance indicating how far (in mm) an apex (located $2q$ ms in time from the initial phase cone) was from the initial site
	distance indicating how far any two consecutive phase cones were from each other
q	number of consecutive time points in a stable phase segment
	1 x q vector demarcating each stable phase segment
	time in milliseconds beginning at window w and extending to window $w + q$
s	phase segment index
	record index
	number of segments per record (r)
	histogram of phase segments
S	EEG phase velocity in $M \text{ sec}^{-1}$
b	slope of the conic surface regressed onto the phase distributio
D	modal diameter in cm - defined as twice the distance from the apex to the half-power point (the square of cosine $45^\circ = 0.5$) of the EEG

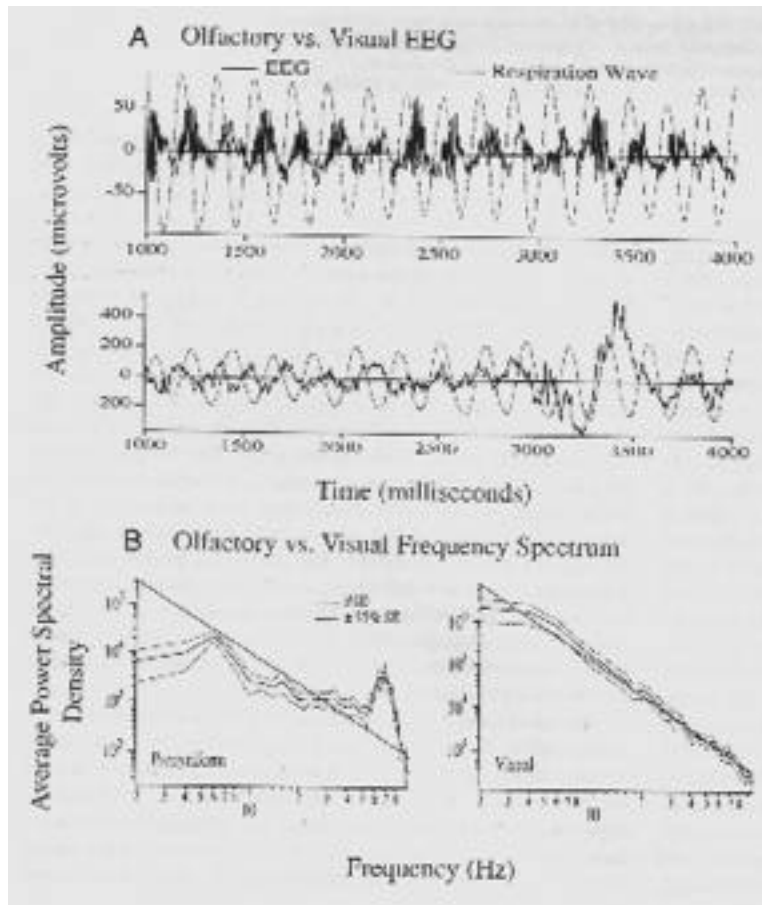
	Visual (n=6)	Somatic (n=6)	Auditory (n=6)
AVG/SD Phase Velocity (M/sec)			
A. 20-40 Hz	0.67 / 0.08	1.19 / 0.54	0.95 / 0.23
B. 40-60 Hz	1.05 / 0.06	2.03 / 0.99	1.59 / 0.43
C. 60-80 Hz	1.44 / 0.05	2.40 / 1.16	2.31 / 0.79
A-C	+ 119 %	+ 99 %	+ 139 %
AVG/SD Modal Diameter (cm)			
A. 20-40 Hz	0.60 / 0.06	0.98 / 0.41	0.84 / 0.19
B. 40-60 Hz	0.55 / 0.03	0.99 / 0.45	0.80 / 0.23
C. 60-80 Hz	0.52 / 0.01	0.84 / 0.40	0.81 / 0.25
A-C	- 13 %	- 16 %	- 4 %

TABLE 1

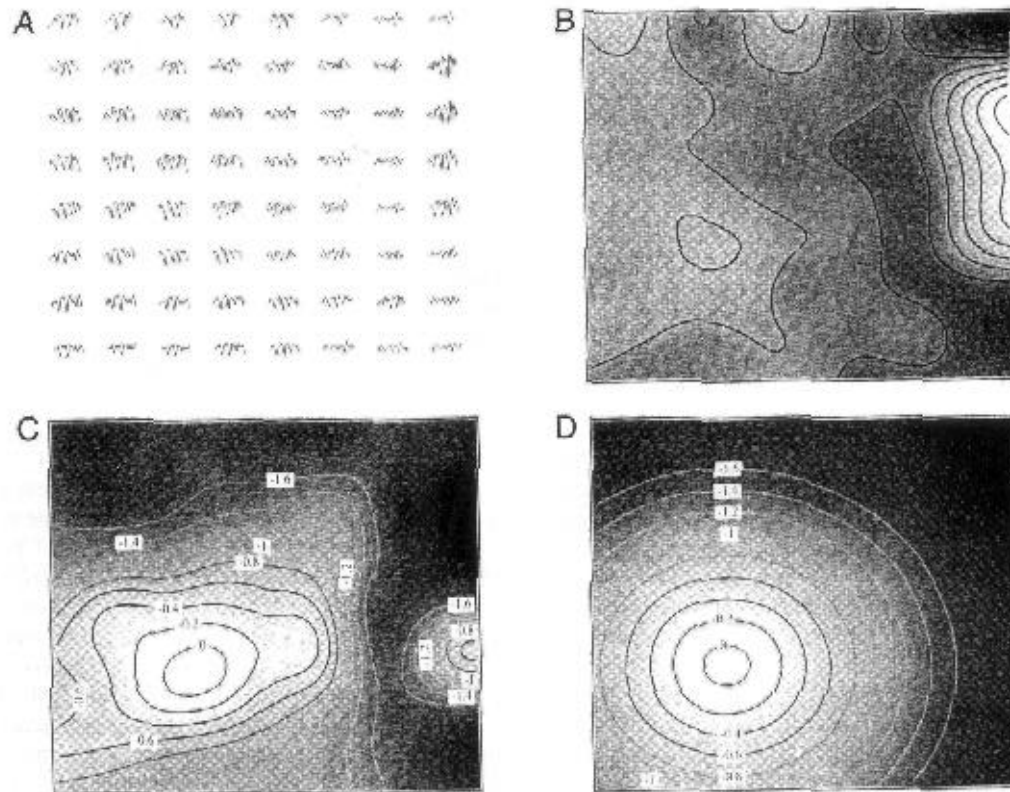
Summary statistics for the average and standard deviation modal phase velocity (M/sec) and modal phase cone diameter (cm) for three different frequency ranges (**a**, 20-40 Hz; **b**, 40-60 Hz; **c**, 60-80 Hz). The percentage of change of the modal values between the first and last frequency ranges is also expressed. Each AVG/SD modal value, for a particular cortical area, was calculated by locating stable phase segments from 18 different experiments using animals with visual, somatic or auditory implants. This table illustrates that the phase velocity increases relative to the frequency of the phase cone, while the conic diameter remains an invariant across frequencies.

**FIGURE 1**

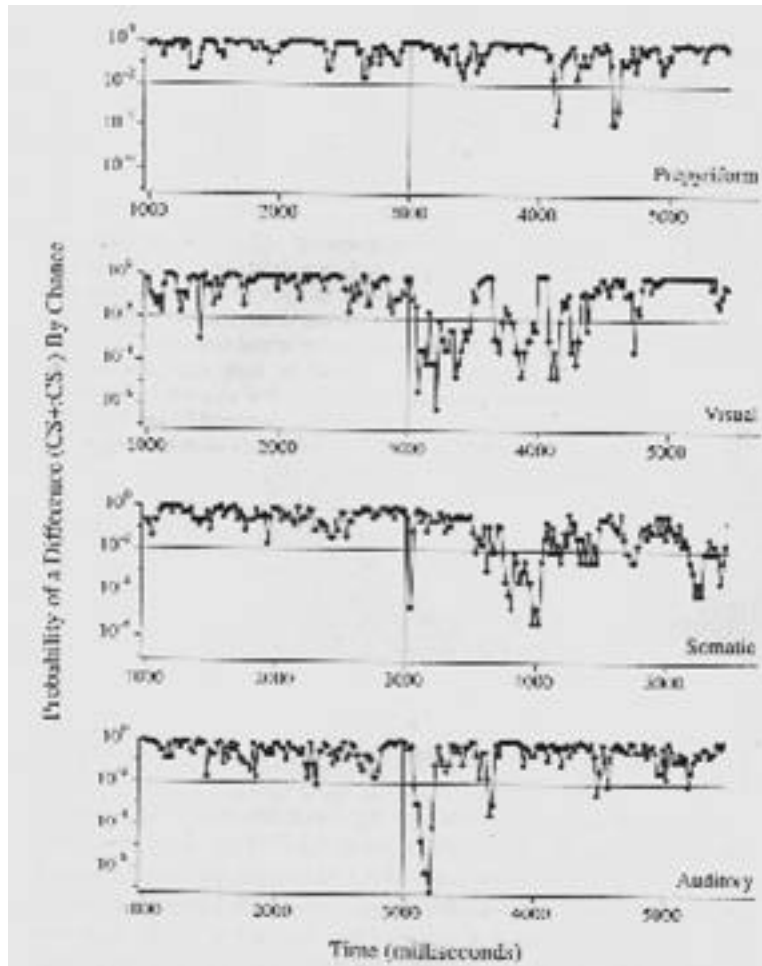
This graph illustrates calculation of a spatial filter tuning curve. The real and imaginary components of the FFT decomposition were iteratively spatially lowpass filtered using different highcut filter settings, with the criterion of the number of post-stimulus (3000-3300 ms) stable phase segments (40+ ms in length) in a 40 record experiment. The count for no filter was 12. Values were optimized in the range of 0.2 to 0.5 cycles/mm. These settings were used for each experiment analyzed. The peak with the highcut spatial filter set at 0.029 cycles/mm was interpreted as an artifact.

**FIGURE 2**

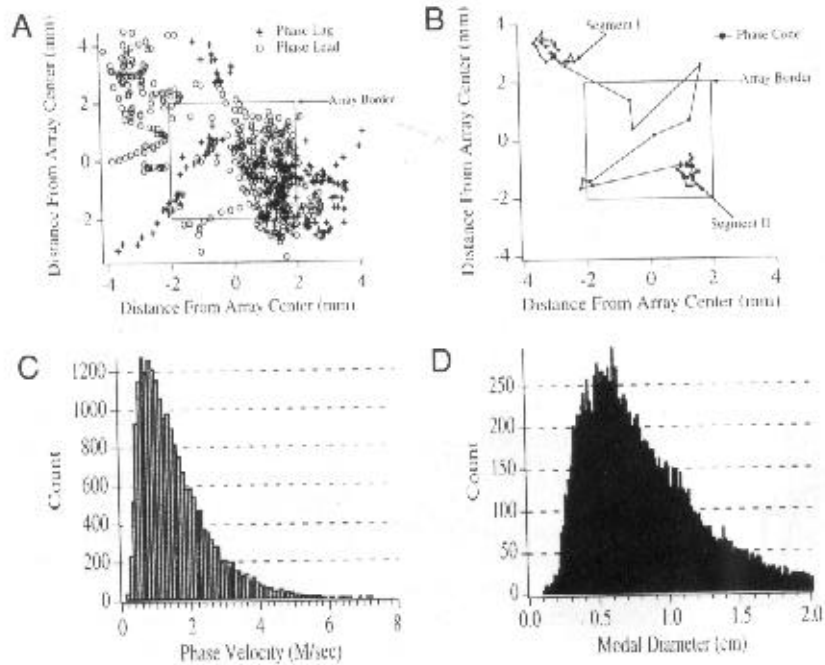
a, These traces represent single channel EEG recordings (solid) and respiratory rhythms (dashed) from a one record of a classical conditioning experiment from the prepyriform cortex (PPC, upper) and the visual cortex (lower). The olfactory trace illustrates a series of high frequency EEG bursts time-locked to the respiration. The visual trace does not show any periodic oscillatory activity, but it does have an evoked potential marking the arrival of the stimulus, $t = 3000$ ms (Barrie et al. 1996). **b**, Temporal frequency spectra. These are averaged frequency spectra (solid traces) and confidence intervals (dashed) from the PPC (left) and visual (right) cortices. Each spectra was averaged across 40 records from a Hamming smoothed, 500 ms post-stimulus window. Regression curves (solid lines) of the form $1/f$ were fit to the 10-50 Hz and 20-80 Hz regions of the PPC and visual spectras, respectively. These figures illustrate that there was an excess of neuroactivity in the 50-80 Hz band of the PPC spectra although the power in the visual EEG was uniformly distributed as $1/f$ across the entire frequency range (Barrie et al. 1996).

**FIGURE 3**

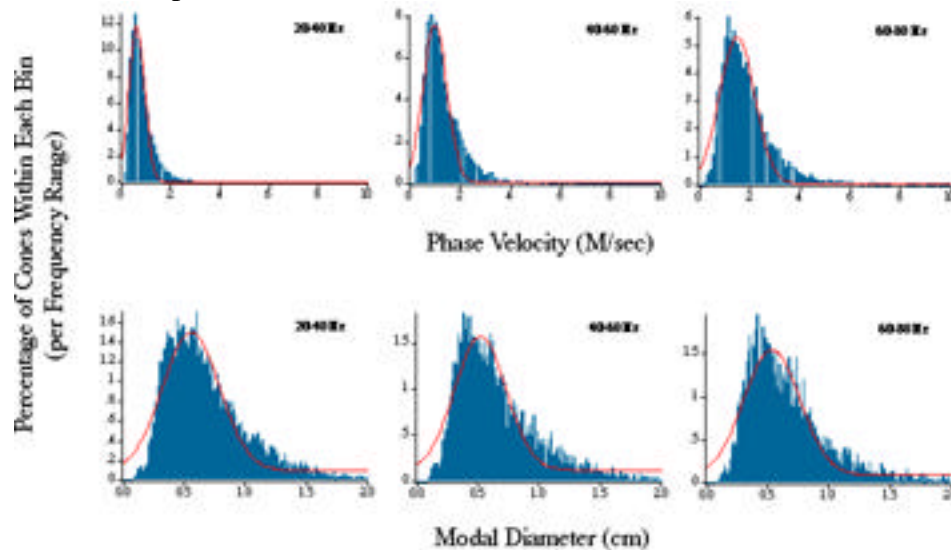
a, Example of one 128 ms EEG segment from visual cortex illustrating amplitude modulation (AM) of the common wave form on 64 channels, temporally filtered (20-80 Hz band pass). **b**, Pattern of RMS amplitude from **(a)**. **c**, Spatially filtered (0.03 - 0.5 cycles/mm band pass) phase distribution at 22 Hz from the FFT of **(a)**. **d**, Regression of a conic surface onto the phase distribution in **(c)** yielding a phase cone with a phase velocity of 0.25 m/s and a half-power diameter of 0.29 cm. The isophase contours (**c-d**) are at intervals of 0.2 radian (11.4°).

**FIGURE 4**

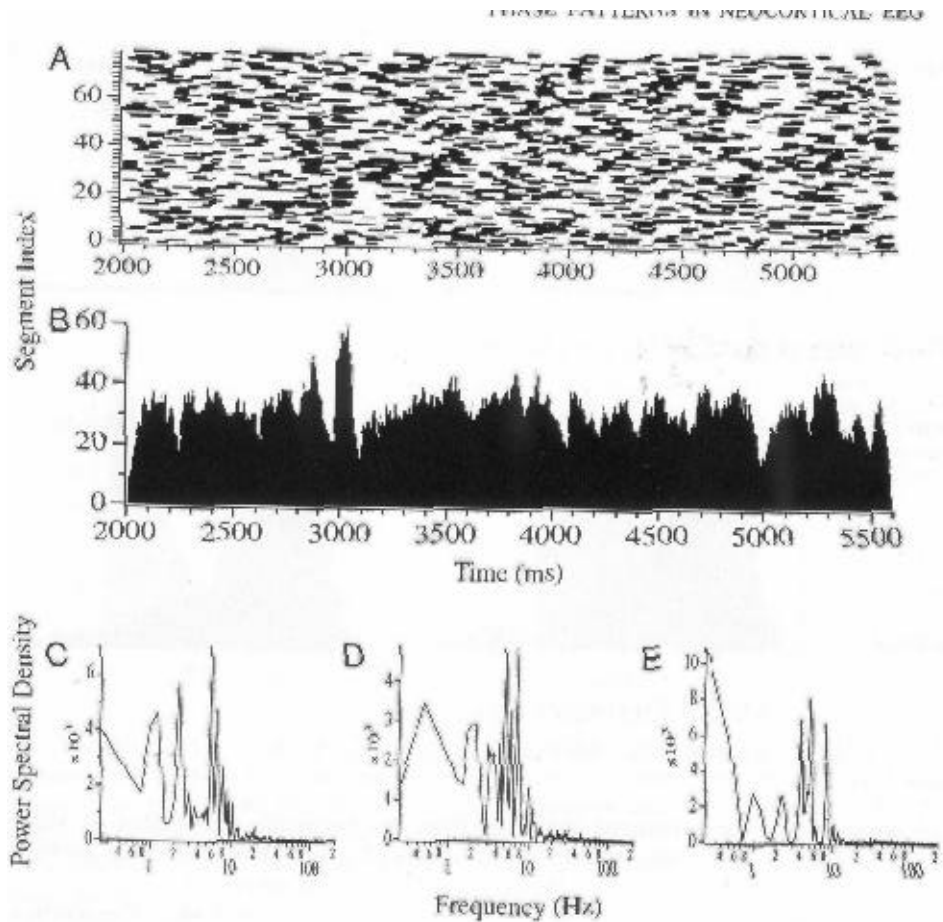
Validation of the significance of spatial AM patterns in EEGs depends on showing that they change with learning (Gray et al. 1986), and EEG segments can be classified with respect to conditioned stimuli that are reinforced (CS+) or not (CS-) on randomly alternated trials. The graph shows estimates of the probability that the degree of correct classification could have occurred by chance, when comparisons are made using a 128 ms window stepped at 2 ms along the 6 second recording period in 20 trials of each stimulus (Freeman and Baird 1987).

**FIGURE 5**

a, Locations of apices of phase cones are projected onto the visual neocortical surface with the 64-channel recording array (square). Each point represents an apex from one phase cone at a best frequency. **b**, Clusters formed when the next apex, 2 ms later, was < 1.2 mm from the site of initial detection, < 0.5 mm from the preceding apex, and had the same sign (lead or lag). The minimum duration was 48 ms; few exceeded 100 ms. A pattern of transition is illustrated as 'Segment I' and 'Segment II.' **c**, Distribution of phase velocities from pooled segments. **d**, Distribution of half-power diameters.

**FIGURE 6**

The visual cortical phase velocities (upper frames) and modal diameters (lower frames) are shown for three frequency ranges. Similar distributions were observed in the auditory and somatic EEGs.



FIGURE

7

a. Solid bars show phase cones stable for >48 ms in 40 trials. When the EEG within a certain time window is decomposed into phase patterns, there is one pattern per frequency bin. Because it was observed that there are often two conic-like patterns of phase existing within the same temporal window at different frequencies, the trial number is half the number on the ordinate to display overlapping segments at different frequencies. We explain the sustained level of incidence in the occurrence of phase cones by inferring that perceptual processes occur before as well as after the presentation of a CS, and that any brain activity pattern that is related to or underlies perception must be found in both prestimulus and poststimulus segments. **b.** Histograms of the above segments. **c-e.** Spectra of the above histograms from the visual (above), somatic, and auditory sessions.

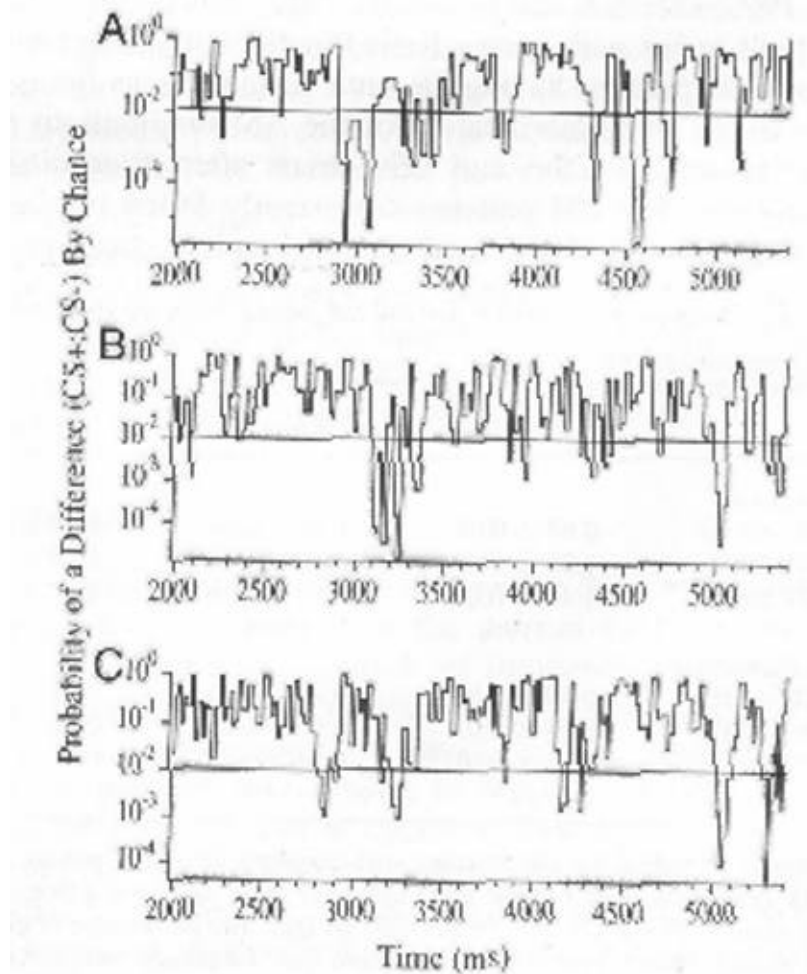


FIGURE 8

The probability of correct classification of AM patterns on discriminative CS+ and CS- trials by chance is shown as time series for the visual, auditory and somatic EEGs over the 6 second duration of the trials, as in Fig. 4. In this figure the EEG segments in which the AM patterns were found were determined from the presence in the window of a stable phase cone in the (a) visual, (b) somatic, and (c) auditory sessions.

REFERENCES

- 1 Abeles, M. *Corticomics: Neural Circuits of the Cerebral Cortex*. Cambridge, UK: Cambridge University Press, 1991.
- 2 Adey, W.R. Slow electrical phenomena in the central nervous system. *Neurosciences Research Program Bulletin*, 1969, **71**: 75-180.
- 3 Adey, W.R. Biological effects of electromagnetic fields. *Journal of Cellular Biochemistry*, 1993, **51**, N4: 410-416.
- 4 Aertsen, A.M., Gerstein, G.L., Habib, M.K. and Palm, G. Dynamics of neuronal firing correlation: modulation of "effective connectivity". *Journal of Neurophysiology*, 1989, **61**: 900-17.
- 5 Amit, D.J. *Modeling Brain Function: The World of Attractor Neural Networks*. Cambridge, UK: Cambridge University Press, 1989.

- 6 Arieli, A., Shohan, D., Hildesheim, R. and Grinvald, A. Coherent spatiotemporal patterns of ongoing activity revealed by real-time optical imaging coupled with single-unit recording in the cat visual cortex. *Journal of Neurophysiology*, 1995, **73**, N4: 2072-2093.
- 7 Barrie, J.M., Freeman, W.J. and Lenhart, M.D. Spatiotemporal analysis of prepyriform, visual, auditory, and somesthetic surface EEGs in trained rabbits. *Journal of Neurophysiology*, 1996, **76**: 520-539.
- 8 Boudreau, J.C. and Freeman, W.J. Spectral analysis of electrical activity in the prepyriform cortex of the cat. *Experimental Neurology*, 1963, **8**: 423-430.
- 9 Braitenberg, V. and Schüz, A. *Anatomy of the Cortex: Statistics and Geometry*. Berlin: Springer-Verlag, 1991.
- 10 Bressler, S.L. Relation of olfactory bulb and cortex. I. Spatial variation of bulbocortical interdependence. *Brain Research*, 1987, **409**: 285-293.
- 11 Bressler, S.L. Large-scale cortical networks and cognition. *Brain Research Reviews*, 1995, **20**: 288-304.
- 12 Brosch, M., Bauer, R. and Eckhorn, R. Synchronous high-frequency oscillations in cat area 18. *European Journal of Neuroscience*, 1995, **7**: 86-95.
- 13 Bullock, T.H. Signals and signs in the nervous system: The dynamic anatomy of electrical activity is probably information-rich. *Proceedings of the National Academy of Sciences, Washington D.C.*, 1997, **94**:1-6
- 14 Bullock, T.H., McClune, M.C., Achimowicz, J.Z., Iraguimadoz, V.J., et al. EEG coherence has structure in the millimeter domain - subdural and hippocampal recordings from epileptic patients. *Electroencephalography and clinical Neurophysiology*, 1995, **95**: 161-177.
- 15 Bures, J., Buresová, O. and Krivánek, J. *The Mechanism and Applications of Leão's Spreading Depression of Electroencephalographic Activity*. New York: Academic Press, 1974.
- 16 Eckman, F.H. and Freeman, W.J. Correlations between unit firing and EEG in the rat olfactory system. *Brain Research*, 1990, **528**: 238-244.
- 17 Elul, R. The genesis of the EEG. *International Review of Neurobiology*, 1972, **15**: 227-272.
- 18 Emery, J. D. and Freeman, W. J. Pattern analysis of cortical evoked potential parameters during attention changes. *Physiology & Behavior*, 1969, **4**: 67-77.
- 19 Engel, A.K., König, P., Kreiter, A.K., Schillen, T.B. and Singer, W. Temporal coding in the visual cortex: new vistas on integration in the nervous system. *Trends in Neuroscience*, 1992, **15**: 218-26.
- 20 Freeman, W.J. Cinematic display of spatial structure of EEG and averaged evoked potentials (AEPs) of olfactory bulb and cortex. *Electroencephalography and clinical Neurophysiology*, 1973, **37**: 199.
- 21 Freeman, W. J. (1962) Comparisons of thresholds for behavioral and electrical responses to cortical electrical stimulation in cats. *Experimental Neurology* **6**: 315-331.
- 22 Freeman, W.J. *Mass Action in the Nervous System*. New York: Academic Press, 1975.
- 23 Freeman, W.J. Spatial properties of an EEG event in the olfactory bulb and cortex. *Electroencephalography and clinical Neurophysiology*, 1978, **44**: 586-605.
- 24 Freeman, W.J. On the problem of anomalous dispersion in chaoto-chaotic phase transitions of neural masses, and its significance for the management of perceptual information in brains. In: *Synergetics of Cognition*, edited by H. Haken and M. Stadler. Berlin: Springer-Verlag, 1990, pp. 126-143.
- 25 Freeman, W.J. The physiology of perception. *Scientific American*, 1991, **264**: 78-85.
- 26 Freeman, W.J. Tutorial on neurobiology: from single neurons to brain chaos. *International Journal of Bifurcation and Chaos*, 1992, **2**: 451-482.
- 27 Freeman, W. J. (1999) Noise-induced first-order phase transitions in chaotic brain activity. *International Journal of Bifurcation and Chaos*, 1999, **9**: 2215-2218.

- 28 Freeman, W. J. *Neurodynamics. An Exploration of Mesoscopic Brain Dynamics*. London UK: Springer-Verlag, 2000.
- 29 Freeman, W.J. and Baird, B. Relation of olfactory EEG to behavior: spatial analysis. *Behavioral Neuroscience*, 1987, **101**: 393-408.
- 30 Freeman, W. J. and Baird, B. (1989) Effects of applied electric current fields on cortical neural activity. Chapter in: Schwartz E (ed.) *Computational Neuroscience*. New York, Plenum Press. pp. 274-287.
- 31 Freeman, W.J., Barrie, J.M., Lenhart, M.D. and Tang, R.X. Spatial phase gradients in neocortical EEGs give modal diameter of 'binding' domains in perception. *Society for Neuroscience Abstracts*, 1995, **21**: 1649.
- 32 Freeman, W. J., Rogers, L. J., Holmes, M. D. and Silbergeld, D. L. (1999) Spatial spectral analysis of human electrocorticograms including the alpha and gamma bands. *Journal of Neuroscience Methods* **90**: 87-95.
- 33 Freeman, W.J. and Schneider, W. Changes in spatial patterns of rabbit olfactory EEG with conditioning to odors. *Psychophysiology*, 1982, **19**: 44-56.
- 34 Freeman, W.J. and Viana Di Prisco, G. Relation of olfactory EEG to behavior: time series analysis. *Behavioral Neuroscience*, 1986, **100**: 753-763.
- 35 Galli, F., Lifschitz, W. and Adrian, H. Studies on the auditory cortex of rabbit. *Experimental Neurology*, 1971, **30**: 324-335.
- 36 Gould, H.J. Body surface maps in the somatosensory cortex of rabbit. *Journal of Comparative Neurology*, 1986, **243**: 207-233.
- 37 Gray, C.M. Synchronous oscillations in neuronal systems: mechanisms and functions. *Journal of Comparative Neuroscience*, 1994, **1**: 11-38.
- 38 Gray, C.M., Freeman, W.J. and Skinner, J.E. Chemical dependencies of learning in the rabbit olfactory bulb: acquisition of the transient spatial pattern change depends on norepinephrine. *Behavioral Neuroscience*, 1988, **100**: 585-596.
- 39 Hameroff, S. Quantum computation in brain microtubules? The Penrose-Hameroff 'Orch OR' model of consciousness. *Philosophical Transactions of the Royal Society of London, Series A-Mathematical, Physical and Engineering Sciences*, 1998, **356**, N1743: 1869-1896.
- 40 Hardcastle, V.G. Psychology's binding problem and possible neurobiological solutions. *Journal of Consciousness Studies*, 1994, **1**: 66-90.
- 41 Hellwig, B. How the myelin picture of the human cerebral cortex can be computed from cytoarchitectural data. A bridge between von Economo and Vogt. *Journal für Hirnforschung*, 1993, **34**: 387-402.
- 42 Hodgkin, A. L. and Rushton, W. A. H. Electrical constants of a crustacean nerve fiber. *Proceedings of the Royal Society (London)*, 1946, **133B**: 444-479.
- 43 Hollander, H. and Halbig, H. Topography of retinal representation in the rabbit cortex: an experimental study using transneuronal and retrograde tracing techniques. *Journal of Comparative Neurology*, 1980, **193**: 701-710.
- 44 Hughes, A. and Vaney, D.I. The organization of binocular cortex in the primary visual area of the rabbit. *Journal of Comparative Neurology* **204**: 151-164, 1982.
- 45 Izus, G. G, Deza, R.R. and Wio, H. S. Exact nonequilibrium potential for the FitzHugh-Nagumo model in the excitable and bistable regimes. *Physical Review E*, 1998, **58**, N1: 93-98.
- 46 Jagadeesh, B., Gray, C.M. and Ferster, D. Visually evoked oscillations of membrane potential in cells of cat visual cortex. *Science*, 1992, **257**, N5069: 552-554.
- 47 König, P. and Schillen, T.B. Stimulus-dependent assembly formation of oscillatory responses: I. Synchronization. *Neural Computation*, 1991, **3**: 155-166.
- 48 Langdon, R.B. and Sur, M. Components of field potentials evoked by white matter stimulation in isolated slices of primary visual cortex: spatial distributions and synaptic order. *Journal of Neurophysiology*, 1990, **64**: 1484-1501.

- 49 Llinás, R. and Ribary, U. Coherent 40-Hz oscillation characterizes dream state in humans. *Proceedings of the National Academy of Sciences, Washington D.C.*, 1993, **90**, N5:2078-2081.
- 50 Lohmann, H. and Roerig, B. Long-range horizontal connections between supragranular pyramidal cells in the extrastriate visual cortex of the rat. *Journal of Comparative Neurology*, 1994, **344**: 543-558.
- 51 McMullen, N.T. and Glaser, E.M. Tonotopic organization of rabbit auditory cortex. *Experimental Neurology*, 1982, **75**: 208-220.
- 52 Milner, P.M. A model for visual shape recognition. *Psychological Review*, 1974, **81**: 521-35.
- 53 Mitzdorf, U. Current source-density method and application in cat cerebral cortex: investigation of evoked potentials and EEG phenomena. *Physiological Reviews*, 1985, **65**: 37-100.
- 54 Mitzdorf, U. Properties of the evoked potential generators: current source-density analysis of visually evoked potentials in the cat cortex. *International Journal of Neuroscience*, 1985, **33**: 33-59, 1987.
- 55 Nicolelis, M. A. L. Beyond maps: The dynamic and distributed organization of the rat somatosensory system. *Somatosensory and Motor Research*, 1997, **14**, N1:63-64.
- 56 Nicolelis, M. A. L., Ghazanfar, A. A. A., Stambaugh, C. R., Oliveira, L. M.O., Laubach, M., Chapin, J. K., Nelson, R.J. and Kaas, J. H. (1998) Simultaneous encoding of tactile information by three primate cortical areas. *Nature Neuroscience*, 1998, **1**: 621-630.
- 57 Nunez, P.L. *Electric fields of the brain : the neurophysics of EEG* . New York : Oxford University Press, 1981.
- 58 Prechtl, J.C., Bullock, T.H., and Kleinfeld, D. Direct evidence for local oscillatory current sources and intracortical phase gradients in turtle visual cortex. *Proceedings of the National Academy of Sciences, Washington D.C.*, 2000, **97**, N2:877-882.
- 59 Press, W.H., Flannery, B.P., Teukolsky, S.A. and Vetterling, W.T. *Numerical recipes in C*. Cambridge, UK: Cambridge University Press, 1988.
- 60 Rall, W. *The Theoretical Foundation of Dendritic Function: Selected Papers of Wilfrid Rall with Commentaries*. Segev, I., Rinzal, J. and Shepherd, G. M. (eds.) Cambridge MA: MIT Press, 1995.
- 61 Read, H.L., Winer, J.A. and Schreiner, C.E. Corticocortical convergence of short- and long-range projections to physiologically defined subregions of cat primary auditory cortex (A1). *Society for Neuroscience*, 1997, **23**: 2072.
- 62 Roelfsema, P.R., Engel, A.K., König, P. and Singer, W. Visuomotor integration is associated with zero time-lag synchronization among cortical areas. *Nature*, 1997, **385**: 157-61.
- 63 Schillen, T. B. and König, P. Binding by temporal structure in multiple feature domains on an oscillatory neuronal network. *Biological Cybernetics*, 1994, **70**: 397-405.
- 64 Sholl, D.A. *The organization of the cerebral cortex*. London: Methuen - Wiley, 1956.
- 65 Singer, W. Synchronization of cortical activity and its putative role in information processing and learning. *Annual Review of Physiology*, 1993, **55**: 349-74.
- 66 Swadlow, H.A. Efferent neurons and suspected interneurons in motor cortex of the awake rabbit: Axonal properties, sensory receptive fields, and subthreshold synaptic inputs. *Journal of Neurophysiology* , 1994, **71**: 437-453, 1994.
- 67 Swadlow, H.A. and Weyand, T.G. Efferent systems of the rabbit visual cortex: laminar distribution of the cells of origin, axonal conduction velocities, and identification of axonal branches. *Journal of Comparative Neurology*, 1981, **203**: 799-822.
- 68 Terzuolo, C.A. and Bullock, T.H. Measurement of imposed voltage gradient adequate to modulate neuronal firing. *Proceedings of the National Academy of Sciences, Washington D.C.*, 1956, **42**: 687-694.
- 69 Thompson, J.M., Woolsey, C.N. and Talbot, S.A. Visual areas I and II of cerebral cortex of rabbit. *Journal of Neurophysiology* **13**: 277-288, 1950.

- 70 Traub, R. D., Whittington, M. A., Stanford, I. M. and Jefferys, J. G. R. A mechanism for generation of long-range synchronous fast oscillations in the cortex. *Nature*, 1996, **383**: 421-424.
- 71 Tsodyks, M., Kenet, T., Grinvald, A. and Arieli, A. Linking spontaneous activity of single cortical neurons and the underlying functional architecture. *Science*, 1999, **286**: 1943-1946.
- 72 Usher, M., Schuster, H.-G. and Niebur, E. Dynamics of populations of integrate-and-fire neurons, partial synchronization and memory. *Neural Computation*, 1993, **5**: 570-586.
- 73 von der Malsburg, C. How are nervous structures organized? In: *Synergetics of the Brain*, edited by E. Basar, H. Flohr, H. Haken and A. J. Mandell. Berlin: Springer-Verlag, 1983, pp. 238-249.
- 74 Walter, W.G. *The Living Brain*. New York: W.W. Norton and Company, Inc., 1953.
- 75 Zhu, J. J. and Connors, B. W. Intrinsic firing patterns and whisker-evoked synaptic responses of neurons in the rat barrel cortex. *Journal of Neurophysiology*, 1999, **81**, N3:1171-1183.